Available online at www.sciencedirect.com
SCIENCE DIRECT®
Remote Sensing of Environment 103 (2006) 488–496
Remote Sensing of Environment
www.elsevier.com/locate/rse

Infrared sea surface emissivity including multiple reflection effect for isotropic Gaussian slope distribution model

Kazuhiko Masuda *

Meteorological Research Institute, Nagamine, 1-1, Tsukuba, Ibaraki 305-0052, Japan

Received 11 December 2005; received in revised form 19 April 2006; accepted 22 April 2006

Abstract

A method is described for incorporating surface-emitted surface-reflected (SESR) radiation into the calculation of infrared sea surface emissivity. Firstly, the direct emissivity is obtained by ignoring SESR emission. Next, the first order SESR emissivity is obtained by using the direct emission as a radiation source. Finally, the *i*th order SESR emissivity is iteratively obtained by using the $i-1$st order SESR emission.

Computational results are in good agreement with a Monte Carlo calculation, where the SESR emissivity increases from an emission angle of 50° showing a maximum value of about 0.03 at an emission angle of 80°. The direct emissivity is smaller than the measured emissivity by 0.02∼0.03 around a wavelength of 10 μm at an emission angle of 73.5°. By incorporating the SESR emission into the emissivity model, the discrepancy between the computed and the measured emissivity is significantly reduced.

The advantage of the present method over the previous works is that we need not to specify a cutoff angle to differentiate the radiation from the sea and that from the sky for calculating SESR emission. Instead of using a cutoff angle, the probability that radiation originates from the sea is derived from the probability distribution function of sea surface slope. As a result, the uncertainty in the computation of sea surface emissivity attributed to the uncertainty in cutoff angle could be effectively suppressed.
© 2006 Elsevier Inc. All rights reserved.

Keywords: Sea surface emissivity; Multiple reflection; Sea surface temperature

1. Introduction

Infrared sea surface emissivity plays an important role for deriving sea surface temperature from satellite measurements and also it is an essential parameter in radiative transfer models. The emissivity model by Masuda et al. (1988) has been validated by comparing with the emissivity measurements using a high spectral infrared spectrometer (Smith et al., 1996) and it is utilized in radiative transfer models (Clough et al., 2005; Mano & Ishimoto, 2004; Matricardi & Saunders, 1999; Sherlock, 1999).

However, the surface-emitted surface-reflected (SESR) radiation has not been taken into account in their model. As a result, the computed emissivity is underestimated at high emission angles. Actually, a difference by 0.02∼0.03 between the model calculation and the measurements is reported at an emission angle of 73.5° in the 10 μm wavelength region (Smith et al., 1996). Wu and Smith (1997) and Bourlier (2005) pointed out that this deviation from the measurements is caused by the fact that the SESR emission is not included in the calculation.

Watts et al. (1996) and Wu and Smith (1997) used the direct emission as a radiation source to obtain the first order SESR emissivity. In their models, a cutoff angle, which is independent of a surface wind speed, is utilized to represent a critical zenith angle below which the source radiation originates from the sea not from the sky. However, the cutoff angle could be variable with a surface wind speed. The uncertainty in cutoff angle may degrade the accuracy of emissivity calculation. Instead of using a cutoff angle, in this paper, a weighting function, which is derived from the probability distribution function of sea surface slope, is utilized to represent the probability that the source radiation originates from the sea.

Basic equations to calculate sea surface emissivity are summarized in Section 2. A method to incorporate the SESR emission into the emissivity model is described in Section 3.

* Tel.: +81 29 853 8577; fax: +81 29 856 0644.
E-mail address: masuda@mri-jma.go.jp.

0034-4257/$ - see front matter © 2006 Elsevier Inc. All rights reserved.
doi:10.1016/j.rse.2006.04.011

Comparisons with the measurements and with a Monte Carlo calculation are presented in Section 4.

2. Basic equations for direct emission from a slope distribution model

Equations for calculating infrared sea surface emissivity, described in Masuda et al. (1988), are summarized in what follows with some modifications.

Fig. 1 shows the geometry of emission from a wave facet tangent to the instantaneous sea surface at point O. $\boldsymbol{i}$ is the unit vector in the direction of emitted radiation which is assumed to be in the $x-z$ plane. $\boldsymbol{n}$ is the facet unit normal vector. $\phi_{\boldsymbol{n}}$ is the azimuth angle of $\boldsymbol{n}$. θ and $\theta_{\boldsymbol{n}}$ are the zenith angles of $\boldsymbol{i}$ and $\boldsymbol{n}$, respectively. The local emission angle to the facet, χ, the slope components, z_x and z_y, are expressed by

$$\cos\chi = \cos\theta\cos\theta_{\boldsymbol{n}} + \sin\theta\sin\theta_{\boldsymbol{n}}\cos\phi_{\boldsymbol{n}}, \tag{1}$$

$$z_x = \partial z/\partial x = -\tan\theta_{\boldsymbol{n}}\cos\phi_{\boldsymbol{n}}, \tag{2}$$

and

$$z_y = \partial z/\partial y = -\tan\theta_{\boldsymbol{n}}\sin\phi_{\boldsymbol{n}}, \tag{3}$$

respectively. From Eqs. (2) and (3), the slope of a facet is expressed in terms of z_x and z_y as

$$\tan^2\theta_{\boldsymbol{n}} = z_x^2 + z_y^2. \tag{4}$$

The emissivity from the facet is given by

$$\varepsilon(\chi) = 1-(|r_l|^2 + |r_r|^2)/2,$$

where $r_l=(\cos\chi'-n\cos\chi)/(\cos\chi'+n\cos\chi)$ and $r_r=(\cos\chi-n\cos\chi')/(\cos\chi+n\cos\chi')$ (Fresnel formulas), where n is the complex refractive index of sea water. The refraction angle is obtained by $\sin\chi'=(1/n)\sin\chi$ (Snell's law).

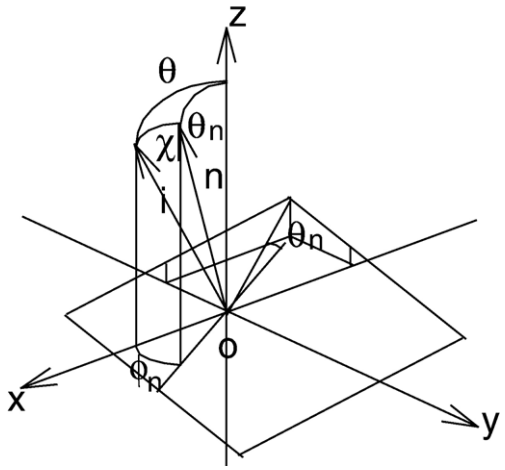

Fig. 1. Geometry of emission from a wave facet tangent to the instantaneous sea surface at point O. $\boldsymbol{i}$ is the unit vector in the direction of emitted radiation which is assumed to be in the $x-z$ plane. $\boldsymbol{n}$ is the facet unit normal vector. $\phi_{\boldsymbol{n}}$ is the azimuth angle of $\boldsymbol{n}$. θ and $\theta_{\boldsymbol{n}}$ are the zenith angles of $\boldsymbol{i}$ and $\boldsymbol{n}$, respectively. χ is the angle of emission with respect to the facet normal.

The distribution of sea surface slope is assumed to obey the isotropic Gaussian function given by Cox and Munk (1955),

$$p(z_x, z_y) = \frac{1}{\pi\sigma^2} e^{-\frac{(z_x^2+z_y^2)}{\sigma^2}} \tag{5}$$

where, $\sigma^2=0.003+0.00512v\pm0.004$. v (m/s) is the wind speed at a height of 12.5 m. The deviation after ± sign is ignored in this paper for simplicity.

Following the formulations by Cox and Munk (1954) and Saunders (1967, 1968), the radiation emitted from a horizontal unit area of wind-roughened sea surface in the direction θ is given by

$$\begin{aligned}&\varepsilon(\theta)B(T_s)\cos\theta\mathrm{d}\Omega\\ &\quad= \int_{-\infty}^{\infty}\int_{-\infty}^{\infty}\varepsilon(\chi)B(T_s)\mathrm{d}\Omega\cos\chi\sec\theta_n P(z_x,z_y)\mathrm{d}z_x\mathrm{d}z_y, \quad \cos\chi>0\end{aligned} \tag{6}$$

where $B(T_s)$ is the black body radiation at surface temperature, T_s. Throughout this study, sea surface is assumed to be isothermal. Then, the sea surface emissivity is expressed by

$$\begin{aligned}\varepsilon(\theta) &= \frac{1}{\cos\theta}\int_{-\infty}^{\infty}\int_{-\infty}^{\infty}\varepsilon(\chi)\cos\chi\sec\theta_{\boldsymbol{n}}P(z_x,z_y)\mathrm{d}z_x\mathrm{d}z_y, \quad \cos\chi>0\\ &= \frac{2}{\cos\theta}\int_0^1\int_0^{\pi}\varepsilon(\chi)\cos\chi P(z_x,z_y)\mu_n^{-4}\mathrm{d}\phi_{\boldsymbol{n}}\mathrm{d}\mu_{\boldsymbol{n}}, \quad \cos\chi>0\end{aligned} \tag{7}$$

Note that integral is performed only for the facets with $\cos\chi>0$. The emissivity computed by Eq. (7), which becomes unbounded as θ approaches 90°, is normalized as

$$\varepsilon^*(\theta) = \varepsilon(\theta)/p(\theta) \tag{8}$$

where

$$\begin{aligned}p(\theta) &= \frac{1}{\cos\theta}\int_{-\infty}^{\infty}\int_{-\infty}^{\infty}\cos\chi\sec\theta_{\boldsymbol{n}}P(z_x,z_y)\mathrm{d}z_x\mathrm{d}z_y, \quad \cos\chi>0\\ &= \frac{2}{\cos\theta}\int_0^1\int_0^{\pi}\cos\chi P(z_x,z_y)\mu_{\boldsymbol{n}}^{-4}\mathrm{d}\phi_{\boldsymbol{n}}\mathrm{d}\mu_{\boldsymbol{n}}, \quad \cos\chi>0\end{aligned} \tag{9}$$

(Masuda et al., 1988).

In the previous paper (Masuda et al., 1988), the normalization is performed from an energy conservation point of view. Later Wu and Smith (1997) pointed out that such a scheme is equivalent to applying the shadowing factor presented by Saunders (1967, 1968). In fact, from Eqs. (1) and (2),

$$\cos\chi = \cos\theta\cos\theta_{\boldsymbol{n}} - \sin\theta\sin\theta_{\boldsymbol{n}}z_x/\tan\theta_{\boldsymbol{n}} = \cos\theta_{\boldsymbol{n}}\cos\theta(1-z_x\tan\theta).$$

Because of $0°\le\theta_{\boldsymbol{n}}<90°$, $\cos\chi>0$ is equivalent to $z_x<\cot\theta$ in the case of $0°\le\theta<90°$ (upward emission). Using $z_x<\cot\theta$, instead of $\cos\chi>0$, Eq. (9) is transformed to $p(\theta)=\frac{1}{\cos\theta}\int_{-\infty}^{\infty}\int_{-\infty}^{\cot\theta}\cos\chi\sec\theta_{\boldsymbol{n}}P(z_x,z_y)\mathrm{d}z_x\mathrm{d}z_y$. Thus, the reciprocal of $p(\theta)$ is the same as the "slope-shadowing factor, S*" which appears in Eq. (6) by Saunders (1968). Note that

Saunders (1968) assumes that all slopes are shadowed with equal frequency. Consequently, S^* is a function of only the emission angle. Hereafter, we denote the shadowing factor as $s(\theta)$.

Suppose that an observer see a horizontal unit area of sea surface from a zenith angle of θ. The area projected onto a plane normal to the line of sight is considered to be $\cos\theta$. $P(z_x,z_y)\mathrm{d}z_x\mathrm{d}z_y$ is the fraction of horizontal unit area of sea surface for which the slope is within the limits $z_x \pm 1/2\mathrm{d}z_x$, $z_y \pm 1/2\mathrm{d}z_y$. The corresponding area projected onto a plane normal to the line of sight is $\cos\chi\sec\theta_n P(z_x,z_y)\mathrm{d}z_x\mathrm{d}z_y$. The integral of this quantity divided by $\cos\theta$ [Eq. (9)] remains unity for example, for emission angles approximately to 80° for $v=1$ m/s and 60° for $v=15$ m/s (Wu & Smith, 1997). It becomes larger than unity for a larger emission angle or wind speed and unbounded as θ approaches 90°. This discrepancy is due to the fact that the hidden areas of wind-roughened sea surface are included in the integration (Wu & Smith, 1997). The shadowing factor, $s(\theta)$, that is the reciprocal of $p(\theta)$, can be interpreted as the ratio of the area projected onto a plane normal to the line of sight that can be actually seen by the observer (i.e. the projected area that is not hidden) to the entire projected area (including the hidden areas) (Saunders, 1968). From a different point of view, $s(\theta)$ can also be interpreted as a probability of emission that is not intercepted by another facet.

3. Surface-emitted surface-reflected radiation

Direct emission can be intercepted by another facet and then reflected into the view direction. This kind of radiation is often referred to as surface-emitted surface reflected (SESR) radiation.

3.1. First order SESR emissivity

A method is proposed by Watts et al. (1996) to estimate the first order SESR by using the direct emission as a radiation source in the slope integral equation. Later, Wu and Smith (1997) improved the model of Watts et al. (1996) by employing an empirical probability function. In this subsection, their models are modified by using a weighting function which is related to the shadowing factor.

Fig. 2 illustrates the geometry of the first order SESR emission that originates from the reflection of direct emission. θ and θ' are the zenith angles of the SESR and the direct emissions, respectively. $\boldsymbol{i}$ and $\boldsymbol{i}'$ are the unit vectors in the directions of the SESR and the direct emissions, respectively. $\boldsymbol{n}$ is the facet unit normal vector. χ is the incident angle with respect to the facet normal. It is shown that $\boldsymbol{n}=(\boldsymbol{i}-\boldsymbol{i}')/(2\cos\chi)$ whereby $\cos\theta'=-2\cos\chi\cos\theta_{\boldsymbol{n}}+\cos\theta$.

To obtain the first order SESR emission, we need to precalculate direct emission in a direction of θ', $\varepsilon^*(\theta')$, where θ' can be equal or larger than 90°. For $\theta' \geq 90°$, Eqs. (7) and (9) may not be suitable because the denominator, $\cos\theta'$, does not make a sense. In such cases, however, $\cos\theta'$ is cancelled out through Eq. (8) and the direct emissivity can be calculated.

Furthermore, we have to determine the probability of direct emission that originates from the sea surface. For $\theta' < 90°$ (upward emission), it is supposed to be unity. For $\theta' \geq 90°$ (downward emission), we focus attention on the backward direction of $\boldsymbol{i}'$, i.e. $-\boldsymbol{i}'$, of which zenith angle is $180°-\theta'$ where $0° \leq 180°-\theta' \leq 90°$. From the discussion in the last paragraph in Section 2, $s(180°-\theta')$ could be interpreted as a probability of the backward trajectory that is not intercepted by another facet, in other words, the probability of emission that originates from the sky. Then, the probability of emission that originates from the sea surface is obtained as $1-s(180°-\theta')$. Such an interpretation of shadowing factor has been presented by Saunders (1967, 1968) to estimate the upper and lower bounds of the effect of multiple reflections on the reflectivity and the emissivity from wind-roughened sea surface. We denote $1-s(180°-\theta')$ as $w(\theta')$ and refer to as a weighting function. In summary, $w(\theta')=1$ for $\theta'<90°$ and $w(\theta')=1-s(180°-\theta')=1-1/p(180°-\theta')$ for $\theta' \geq 90°$.

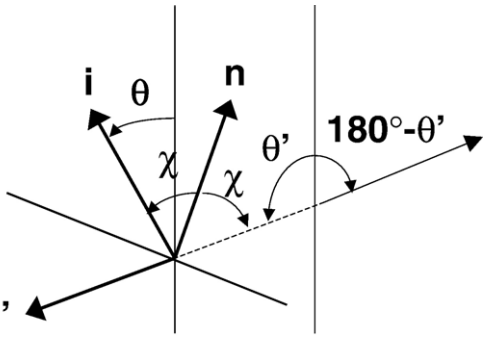

Fig. 2. Figure showing the direction of direct emission (θ'), which is used as a radiation source for obtaining the first order SESR emission into the θ direction. $\boldsymbol{i}$ and $\boldsymbol{i}'$ are the unit vectors in the directions of SESR and direct emissions, respectively. $\boldsymbol{n}$ is the facet unit normal vector. χ is the incident angle with respect to the facet normal.

We substitute $\rho(\chi)\varepsilon^*(\theta')w(\theta')$ for $\varepsilon(\chi)$ in Eq. (7) to obtain the first order SESR emissivity from the reflection of direct emission where the reflectivity, $\rho(\chi)=(|r_l|^2+|r_r|^2)/2$, is obtained from the Fresnel formulas (Section 2).

An example of direct sea surface emissivity, $\varepsilon^*(\theta')$, shadowing factor, $s(\theta')$, and weighting function, $w(\theta')=1-s(180°-\theta')$, are illustrated in Fig. 3 at a wavelength of 11 μm for $v=10$ m/s. Refractive index of pure water by Hale and Querry (1973) is used with the salinity adjustment from Friedman (1969) as in Masuda et al. (1988). The shadowing factor is unity for $\theta'<70°$ and decreases to zero as θ' approaches 90°. The weighting function discontinuously decreases from unity at $\theta'=90°$ and approaches zero approximately at $\theta'=110°$. The direct emissivity decreases monotonously beyond $\theta'=90°$ with increasing θ'.

The scheme in this paper is the same as that in Watts et al. (1996) for $\theta'<90°$ (upward direct emission). Note that, in this paper, the direction of measuring the zenith angle of direct emission is different from Watts et al. (1996); namely, θ_s in Watts et al. (1996) is $180°-\theta'$ in this paper. For $\theta' \geq 90°$ (downward direct emission), Watts et al. (1996) used a cutoff angle (θ_{cutoff}) to differentiate the radiation from the sea and that from the sky. The SESR emissivity is then obtained with $w(\theta')=1$ for $\theta'<\theta_{\mathrm{cutoff}}$ and with $w(\theta')=0$ for $\theta'>\theta_{\mathrm{cutoff}}$. The cutoff angle is expressed as a function of the ratio of the wave height and the wavelength which could vary with a wind speed. A cutoff angle of 95° was selected in Watts et al. (1996) to estimate a realistic maximum effect by SESR emission. Note that the above-mentioned cutoff angle of 95° is equivalent to that of 85° in Watts et al. (1996) for the same reason as mentioned before for the direction of the zenith angle of direct emission. The direct emissions with emission angles larger than this angle are not used to calculate SESR emissivity in the

scheme by Watts et al. (1996). On the other hand, in the present method, the weighting function, $w(\theta')=1-s(180°-\theta')$, decreases continuously for $\theta'\geq 90°$ so that all the pre-calculated direct emission may be utilized by multiplying this function. For example, $\varepsilon^*(\theta')w(\theta')$ are 0.66×0.51 and 0.59×0.12 for $\theta'=92.5°$ and $\theta'=97.7°$, respectively, in the case of Fig. 3.

Wu and Smith (1997) improved the method by Watts et al. (1996) by using a parabolic function between $\theta'=90°$ and the cutoff angle to represent the probability that the direct emission originates from the sea surface. But dependence of the probability function on a surface wind speed has not been taken into account. It is probable that the probability that direct emission originates from the sea is dependent on a surface wind speed because the distribution of sea surface slope is expressed in terms of a surface wind speed. One of the advantages of the present method is that the weighing function is expressed as a function of the surface wind speed by way of the probability distribution function of sea surface slope. Fig. 4 shows the weighting functions, $w(\theta')$, for $v=5$, 10, and 15 m/s, at zenith angles from 90° to 120°. $w(\theta')$ is found to increase with wind speed. This characteristic is quite reasonable because the emitted radiation that originates from the sea surface could increase with roughness of sea surface.

For the first order SESR emission, the equation corresponding to Eq. (7) is

$$r_1(\theta)=\frac{2}{\cos\theta}\int_0^1\int_0^\pi \rho(\chi)\varepsilon^*(\theta')w(\theta')\cos\chi P(z_x,z_y)\mu_n^{-4}\mathrm{d}\phi_n\mathrm{d}\mu_n,\quad \cos\chi>0. \tag{11}$$

Scattering and absorption by the air are ignored in this study for simplicity. Similar to the direct emissivity, $r_1(\theta)$ is normalized as

$$r_1^*(\theta)=r_1(\theta)/p(\theta). \tag{12}$$

3.2. Higher order SESR emissivity

The higher order SESR emissivity could be obtained in a manner similar to the first order SESR emissivity. Suppose that the $i-1$st order SESR emissivity has been obtained as $r_{i-1}^*(\theta)$. For the

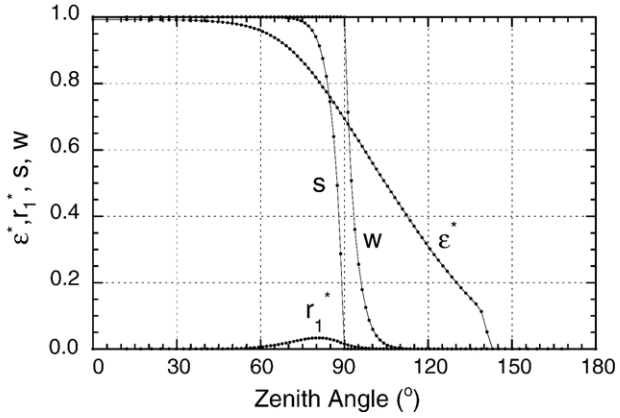

Fig. 3. Direct emissivity, $\varepsilon^*(\theta')$, first order SESR emissivity, $r_1^*(\theta')$, shadowing factor, $s(\theta')$, and weighting function, $w(\theta')=1-s(180°-\theta')$ at a wavelength of 11 μm for $v=10$ m/s as functions of the zenith angle.

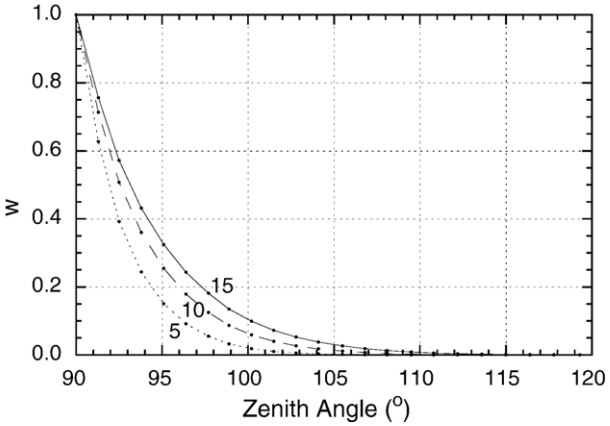

Fig. 4. Weighting function, $w(\theta')$, for $v=5$ m/s (dotted line), 10 m/s (dashed line), and 15 m/s (solid line) at zenith angles from 90° to 120°.

ith order SESR emission ($i\geq 2$), the equation corresponding to Eq. (11) is then

$$r_i(\theta)=\frac{2}{\cos\theta}\int_0^1\int_0^\pi \rho(\chi)r_{i-1}^*(\theta')w(\theta')\cos\chi P(z_x,z_y)\mu_n^{-4}\mathrm{d}\phi_n\mathrm{d}\mu_n,\quad \cos\chi>0 \tag{13}$$

Similar to the first order SESR emissivity, $r_i(\theta)$ is normalized as

$$r_i^*(\theta)=r_i(\theta)/p(\theta). \tag{14}$$

Thus, the higher order SESR emissivities are calculated iteratively. Finally, the surface emissivity including the surface reflection effect is obtained as

$$\varepsilon^*(\theta)+\sum_{i=1}^{\infty} r_i^*(\theta).$$

4. Results and discussion

4.1. Example of sea surface emissivity including SESR radiation

The direct emissivity [$\varepsilon^*(\theta)$], the first and second order SESR emissivities [$r_1^*(\theta)$, and $r_2^*(\theta)$] are shown in Table 1 for three wavelengths, 3.7 μm, 11.0 μm, and 12.0 μm. These results were obtained in two steps as follows.

Step 1 Pre-calculate $w(\theta')$, $\varepsilon^*(\theta')$, and $r_1^*(\theta')$ in the integral of Eqs. (11) and (13) for use in Step 2.

[1-1] $p(\theta')$ is calculated by using Eq. (9) from which $w(\theta')$ is obtained.

[1-2] $\varepsilon^*(\theta')$ is calculated from Eqs. (7) and (8) by using $p(\theta')$.

[1-3] $r_1^*(\theta')$ is calculated from Eqs. (11) and (12) by using $\varepsilon^*(\theta')$, $w(\theta')$, and $p(\theta')$. $\varepsilon^*(\theta')$ and $w(\theta')$ in Eq. (11) are linearly interpolated in μ' space where $\mu'=\cos\theta'$.

$p(\theta')$, $\varepsilon^*(\theta')$, and $r_1^*(\theta')$ were calculated for 91 equally spaced μ' from -1.0 to 1.0. The number of 91 was chosen so that linear interpolation may be

Table 1
Direct emissivity [$\varepsilon^*(\theta)$], first order SESR emissivity [$r_1^*(\theta)$], and second order SESR emissivity [$r_2^*(\theta)$]

Wavelength = 3.7 μm, $n = 1.380 - i0.004$

v(m/s)	0.0	10.0	20.0	30.0	40.0	50.0	60.0	70.0	75.0	80.0	85.0
$\varepsilon^*(\theta)$											
0.0	0.9745	0.9745	0.9743	0.9732	0.9697	0.9594	0.9311	0.8541	0.7751	0.6459	0.4486
1.0	0.9745	0.9745	0.9742	0.9731	0.9695	0.9589	0.9302	0.8537	0.7777	0.6610	0.5073
3.0	0.9745	0.9745	0.9742	0.9729	0.9690	0.9579	0.9284	0.8536	0.7848	0.6904	0.5800
5.0	0.9745	0.9744	0.9741	0.9727	0.9685	0.9569	0.9269	0.8546	0.7931	0.7146	0.6261
10.0	0.9744	0.9743	0.9738	0.9721	0.9672	0.9544	0.9238	0.8599	0.8127	0.7569	0.6954
15.0	0.9744	0.9742	0.9735	0.9714	0.9659	0.9522	0.9218	0.8662	0.8283	0.7847	0.7364
$r_1^*(\theta)$											
0.0	0.0000	0.0000	0.0000	0.0000	0.0000	0.0000	0.0000	0.0000	0.0001	0.0017	0.0147
1.0	0.0000	0.0000	0.0000	0.0000	0.0000	0.0000	0.0000	0.0004	0.0030	0.0127	0.0253
3.0	0.0000	0.0000	0.0000	0.0000	0.0000	0.0000	0.0004	0.0051	0.0135	0.0254	0.0291
5.0	0.0000	0.0000	0.0000	0.0000	0.0000	0.0001	0.0017	0.0111	0.0210	0.0303	0.0295
10.0	0.0000	0.0000	0.0000	0.0000	0.0003	0.0016	0.0073	0.0215	0.0295	0.0336	0.0287
15.0	0.0000	0.0000	0.0000	0.0002	0.0011	0.0042	0.0127	0.0268	0.0325	0.0337	0.0276
$r_2^*(\theta)$											
0.0	0.0000	0.0000	0.0000	0.0000	0.0000	0.0000	0.0000	0.0000	0.0000	0.0001	0.0005
1.0	0.0000	0.0000	0.0000	0.0000	0.0000	0.0000	0.0000	0.0000	0.0001	0.0004	0.0008
3.0	0.0000	0.0000	0.0000	0.0000	0.0000	0.0000	0.0000	0.0002	0.0004	0.0008	0.0008
5.0	0.0000	0.0000	0.0000	0.0000	0.0000	0.0000	0.0000	0.0004	0.0007	0.0009	0.0007
10.0	0.0000	0.0000	0.0000	0.0000	0.0000	0.0000	0.0002	0.0007	0.0009	0.0009	0.0006
15.0	0.0000	0.0000	0.0000	0.0000	0.0000	0.0001	0.0004	0.0008	0.0009	0.0008	0.0005

Wavelength = 11.0 μm, $n = 1.162 - i0.094$

v(m/s)	0.0	10.0	20.0	30.0	40.0	50.0	60.0	70.0	75.0	80.0	85.0
$\varepsilon^*(\theta)$											
0.0	0.9925	0.9925	0.9924	0.9919	0.9902	0.9846	0.9668	0.9088	0.8406	0.7171	0.5108
1.0	0.9925	0.9925	0.9924	0.9919	0.9901	0.9842	0.9659	0.9076	0.8414	0.7299	0.5717
3.0	0.9925	0.9925	0.9924	0.9918	0.9898	0.9835	0.9643	0.9061	0.8456	0.7563	0.6456
5.0	0.9925	0.9925	0.9923	0.9917	0.9895	0.9828	0.9627	0.9057	0.8516	0.7780	0.6911
10.0	0.9925	0.9924	0.9922	0.9913	0.9887	0.9809	0.9594	0.9079	0.8667	0.8158	0.7575
15.0	0.9925	0.9924	0.9920	0.9910	0.9878	0.9791	0.9571	0.9119	0.8792	0.8401	0.7955
$r_1^*(\theta)$											
0.0	0.0000	0.0000	0.0000	0.0000	0.0000	0.0000	0.0000	0.0000	0.0001	0.0018	0.0162
1.0	0.0000	0.0000	0.0000	0.0000	0.0000	0.0000	0.0000	0.0004	0.0030	0.0132	0.0275
3.0	0.0000	0.0000	0.0000	0.0000	0.0000	0.0000	0.0003	0.0047	0.0131	0.0260	0.0311
5.0	0.0000	0.0000	0.0000	0.0000	0.0000	0.0001	0.0014	0.0101	0.0203	0.0307	0.0311
10.0	0.0000	0.0000	0.0000	0.0000	0.0002	0.0011	0.0059	0.0195	0.0281	0.0334	0.0295
15.0	0.0000	0.0000	0.0000	0.0001	0.0007	0.0030	0.0103	0.0242	0.0306	0.0329	0.0279
$r_2^*(\theta)$											
0.0	0.0000	0.0000	0.0000	0.0000	0.0000	0.0000	0.0000	0.0000	0.0000	0.0001	0.0006
1.0	0.0000	0.0000	0.0000	0.0000	0.0000	0.0000	0.0000	0.0000	0.0001	0.0004	0.0009
3.0	0.0000	0.0000	0.0000	0.0000	0.0000	0.0000	0.0000	0.0001	0.0004	0.0008	0.0008
5.0	0.0000	0.0000	0.0000	0.0000	0.0000	0.0000	0.0000	0.0003	0.0006	0.0009	0.0007
10.0	0.0000	0.0000	0.0000	0.0000	0.0000	0.0000	0.0002	0.0006	0.0008	0.0009	0.0006
15.0	0.0000	0.0000	0.0000	0.0000	0.0000	0.0001	0.0003	0.0007	0.0008	0.0008	0.0005

Wavelength = 12.0 μm, $n = 1.118 - i0.190$

v(m/s)	0.0	10.0	20.0	30.0	40.0	50.0	60.0	70.0	75.0	80.0	85.0
$\varepsilon^*(\theta)$											
0.0	0.9889	0.9889	0.9888	0.9880	0.9853	0.9766	0.9506	0.8740	0.7928	0.6589	0.4554
1.0	0.9889	0.9889	0.9887	0.9879	0.9851	0.9761	0.9496	0.8734	0.7953	0.6746	0.5159
3.0	0.9889	0.9889	0.9887	0.9878	0.9846	0.9751	0.9476	0.8730	0.8024	0.7051	0.5911
5.0	0.9889	0.9889	0.9886	0.9876	0.9842	0.9741	0.9459	0.8737	0.8108	0.7300	0.6387
10.0	0.9889	0.9888	0.9884	0.9871	0.9830	0.9716	0.9424	0.8785	0.8305	0.7734	0.7101
15.0	0.9888	0.9887	0.9882	0.9865	0.9818	0.9693	0.9401	0.8846	0.8462	0.8017	0.7523
$r_1^*(\theta)$											
0.0	0.0000	0.0000	0.0000	0.0000	0.0000	0.0000	0.0000	0.0000	0.0001	0.0017	0.0148
1.0	0.0000	0.0000	0.0000	0.0000	0.0000	0.0000	0.0000	0.0004	0.0030	0.0128	0.0255
3.0	0.0000	0.0000	0.0000	0.0000	0.0000	0.0000	0.0003	0.0051	0.0135	0.0256	0.0295

Table 1 (*continued*)

Wavelength = 3.7 μm, $n = 1.380 - i0.004$											
v(m/s)	0.0	10.0	20.0	30.0	40.0	50.0	60.0	70.0	75.0	80.0	85.0
5.0	0.0000	0.0000	0.0000	0.0000	0.0000	0.0001	0.0016	0.0110	0.0210	0.0306	0.0299
10.0	0.0000	0.0000	0.0000	0.0000	0.0002	0.0015	0.0070	0.0213	0.0296	0.0340	0.0291
15.0	0.0000	0.0000	0.0000	0.0002	0.0009	0.0038	0.0122	0.0266	0.0326	0.0340	0.0280
$r_2^*(\theta)$											
0.0	0.0000	0.0000	0.0000	0.0000	0.0000	0.0000	0.0000	0.0000	0.0000	0.0001	0.0006
1.0	0.0000	0.0000	0.0000	0.0000	0.0000	0.0000	0.0000	0.0000	0.0001	0.0004	0.0008
3.0	0.0000	0.0000	0.0000	0.0000	0.0000	0.0000	0.0000	0.0002	0.0004	0.0008	0.0008
5.0	0.0000	0.0000	0.0000	0.0000	0.0000	0.0000	0.0000	0.0003	0.0007	0.0009	0.0007
10.0	0.0000	0.0000	0.0000	0.0000	0.0000	0.0000	0.0002	0.0007	0.0009	0.0009	0.0006
15.0	0.0000	0.0000	0.0000	0.0000	0.0000	0.0001	0.0004	0.0008	0.0009	0.0008	0.0005

performed with sufficient accuracy to obtain SESR emissivity. Simpson's rule is adopted for both zenith and azimuth integrals as in Masuda et al. (1988). The numbers of quadrature points are 51 for $0.5 \le |\mu'| \le 1.0$, 101 for $0.35 \le |\mu'| \le 0.5$, 151 for $0.25 \le |\mu'| \le 0.35$, 301 for $0.15 \le |\mu'| \le 0.25$, and 801 for $0.0 \le |\mu'| \le 0.15$. The lower boundary of zenith integral, μ_n^*, is obtained according to Eq. (23) by Masuda et al. (1988). $\varepsilon^*(\theta')$ and $r_1^*(\theta')$ are illustrated in Fig. 3 at a wavelength of 11 μm for $v = 10$ m/s as an example.

Step 2 Calculate $\varepsilon^*(\theta)$, $r_1^*(\theta)$, and $r_2^*(\theta)$ at the emission angles specified in Table 1.

[2-1] $p(\theta)$ is calculated from Eq. (9).

[2-2] $\varepsilon^*(\theta)$ is calculated from Eqs. (7) and (8) by using $p(\theta)$.

[2-3] $r_1^*(\theta)$ is calculated from Eqs. (11) and (12) by using $w(\theta')$ and $\varepsilon^*(\theta')$ pre-calculated in Step 1 and $p(\theta)$.

[2-4] $r_2^*(\theta)$ is calculated from Eqs. (13) and (14) by using $w(\theta')$ and $r_1^*(\theta')$ pre-calculated in Step 1 and $p(\theta)$.

Number of quadrature points and lower boundary in zenith integral are the same as Step 1.

From Table 1, it is found that the computed sea surface emissivity converges by taking the first and second order SESR emissions into account. The first order SESR emissivity is less than 0.005 for emission angles less than 50°. It increases with increasing emission angle showing the maximum about 0.03 at 80°. It is also shown that the first order SESR emissivity increases with surface wind speed except for $\theta = 85°$.

4.2. Comparison of SESR emissivity with Monte Carlo calculation

Fig. 5 compares the SESR emissivity calculated by the present method with that obtained by a Monte Carlo calculation at a wavelength of 4 μm for $v = 5$, 10, and 15 m/s. The plots for the Monte Carlo results are reproduced from Fig. 6 by Henderson et al. (2003). They used the two-dimensional Gaussian distribution model (Cox & Munk, 1954) whereas we adopted the isotropic Gaussian distribution model (Cox & Munk, 1955). Therefore, we cannot expect a perfect agreement between the results. Nevertheless, the general trends of SESR emissivity described in Subsection 4.1 are observed in both models. Note that Henderson et al. (2003) considered up to the tenth order SESR emissivity whereas we considered up to the second order SESR emissivity. As mentioned in Section 4.1, however, the SESR emissivity could converge by taking up to the second order SESR emissivity. The difference in the SESR emissivity between two methods is not attributed to the number of reflections.

4.3. Comparison of SESR emissivity with calculation using cutoff angle

The influence of cutoff angle on the SESR emissivity is investigated in Fig. 6 at a wavelength of 4 μm for $v = 5$ m/s and 15 m/s where cutoff angles of 90°, 95°, and 100° are taken into account. In this calculation, the downward radiation in directions larger than the cutoff angle is omitted in the integral of Eqs. (11) and (13) whereas that in the directions less than the cutoff angle is integrated with a weighting function of $w(\theta') = 1$. Note that this treatment is equivalent to the scheme presented by Watts et al. (1996). As seen in Fig. 6, the SESR emissivity increases with cutoff angle. For a comparison purpose, the SESR emissivity calculated

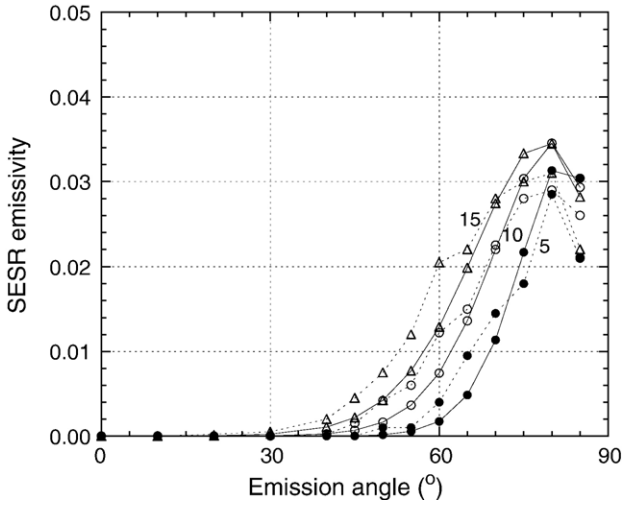

Fig. 5. Comparison of the SESR emissivity calculated by the present method (solid lines) with that calculated by a Monte Carlo method (dotted lines) at a wavelength of 4 μm for $v = 5$ m/s (filled circles), 10 m/s (open circles), and 15 m/s (triangles). Results of the Monte Carlo method are reproduced from Fig. 6 by Henderson et al. (2003).

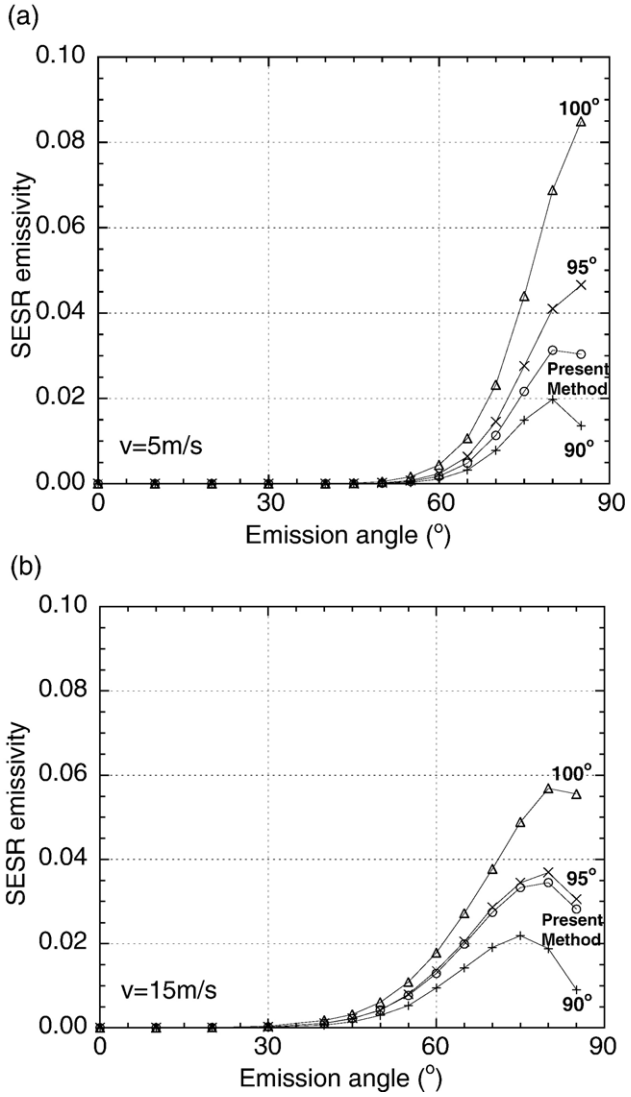

Fig. 6. Influence of a cutoff angle on the SESR emissivity at a wavelength of 4 μm for (a) $v=5$ m/s and (b) $v=15$ m/s for cutoff angles of 90° (pluses), 95° (crosses), and 100° (triangles). The SESR emissivity calculated by the present method is plotted for a comparison purpose (open circles). See text for the definition of cutoff angle.

by the present method with a weighting function of $1-s(180°-\theta')$ is plotted. Model computations of SESR emissivity with this weighing function are most consistent with those with the cutoff angle of 95° for both wind speeds.

It should be noted that a difference of 5° in cutoff angle causes the SESR emissivity fluctuation approximately by 0.01~0.02 at the 75° emission angle. The accuracy of cutoff angle is essential to obtain SESR emissivity precisely. As mentioned earlier, the present method is useful to eliminate the error in the computed SESR emissivity arising from the uncertainty of cutoff angle.

4.4. Comparison of the sea surface emissivity with measurement

Fig. 7(a) shows a comparison of the direct emissivity, for selected eight wavelengths, calculated from Eq. (8) with the emissivity determined from the measurement by using a high

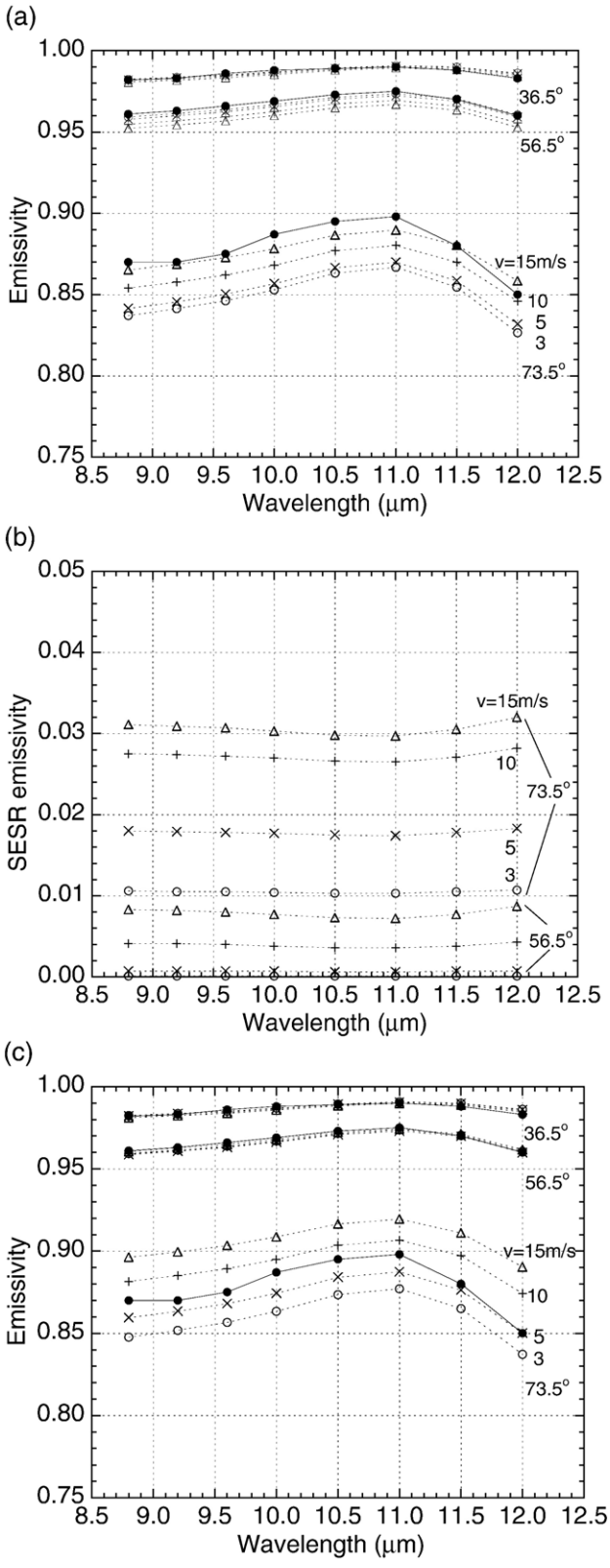

Fig. 7. (a) Comparison of the direct emissivity calculated from Eq. (8) with the measurements at emission angles of 36.5°, 56.5°, and 73.5°. The measured emissivities (filled circles) are reproduced from Fig. 10 by Smith et al. (1996). Calculations are plotted for $v=3$ m/s (open circles), 5 m/s (crosses), 10 m/s (pluses), and 15 m/s (triangles). (b) SESR emissivities at emission angles of 56.5° and 73.5°. SESR emissivity for 36.5° is negligibly small. (c) Same as (a) but for the emissivity including the SESR emission.

spectral resolution infrared radiometer aboard an oceanographic research vessel (Smith et al., 1996). The plots of emissivity measurements are reproduced from Fig. 10 by Smith et al. (1996). Model calculation at the 36.5° emission angle is consistent with the measurements. For the 56.5° emission angle, the model calculation with $v=3$ m/s is consistent with the measurements whereas that with $v=15$ m/s is smaller than the measurements approximately by 0.01. For the 73.5° emission angle, the model calculation is smaller than the measurements approximately by 0.01 for $v=15$ m/s and by 0.03 for $v=3$ m/s.

Fig. 7(b) shows the SESR emissivity up to the second order for emission angles of 56.5° and 73.5°. The SESR emissivity at an emission angle of 36.5° is negligibly small (Table 1). The SESR emissivity increases with wind speed for both emission angles. It reaches to 0.01 and 0.03 at $v=15$ m/s for emission angles of 56.5° and 73.5°, respectively.

Fig. 7(c) is the same as Fig. 7(a) except that the emissivity including the SESR emission is compared with the measurements. The model calculation is much improved by taking the SESR emissivity into account. For the 56.5° emission angle, the agreement between the model calculation and the measurement is excellent. For the 73.5° emission angle, the computed emissivity ignoring SESR emission is smaller than the measurements [Fig. 7(a)] for all the wind speed considered. The wind speed on the day data were taken is reported as 5 m/s (Wu & Smith, 1997) and between 3 m/s and 9 m/s (Henderson et al., 2003). By including the SESR emission, the measurement is between the model calculations for $v=5$ m/s and $v=10$ m/s [Fig. 7(c)]. From these results, we can conclude that the discrepancy between the measurements and the calculations is much reduced by taking the SESR emission into account.

We next examine the dependence of sea surface emissivity on surface wind speed. The direct emissivity decreases with wind speed at an emission angle of 56.5° but increases with wind speed at 73.5° [Fig. 7(a)]. By including the SESR emission, wind speed dependence of sea surface emissivity becomes larger at the 73.5° emission angle whereas emissivity at 56.5° seems to show almost the same value for all the wind speed [Fig. 7(c)]. From the measurement of sea surface emissivity, Hanafin and Minnett (2005) found that the emissivity increase with increasing wind speed at an emission angle of 55°. For example, average emissivies observed at wind speed ranges of 0∼1 m/s, 4∼5 m/s, 8∼9 m/s, and 12∼13 m/s, are respectively, 0.978, 0.982, 0.982, and 0.982 (Table 5 in Hanafin and Minnett, 2005) at a wavelength of 11 μm. The emissivities obtained by the present method with the SESR emission were 0.978, 0.976, 0.975, and 0.976, respectively, for wind speeds of 0.5 m/s, 4.5 m/s, 8.5 m/s, and 12.5 m/s, at a wavelength of 11 μm. For a calm condition, the measured and the calculated sea surface emissivities are consistent with each other. The measured emissivity slightly increases by 0.004 while the calculated emissivity slightly decreases by 0.002 with changing of wind speed from 0 m/s to 5 m/s. In the wind speed range from 5 m/s to 13 m/s, both the observed and the calculated emissivities show almost constant values with a bias of about 0.006. The emissivities calculated by ignoring the SESR emission were 0.978, 0.976, 0.974, and 0.972, respectively, for wind speeds of 0.5 m/s, 4.5 m/s, 8.5 m/s, and 12.5 m/s. In this case, sea surface emissivity decreases monotonously with the increasing wind speed. By including the SESR emission, the calculated emissivity approaches the observation.

5. Conclusions

The present method is based on the models by Watts et al. (1996) and Wu and Smith (1997) for incorporating the surface-emitted surface-reflected (SESR) radiation into the calculation of infrared sea surface emissivity. In their models, a cutoff angle has to be specified in advance to differentiate the radiation from the sea and that from the sky to obtain SESR emissivity. It is probable that the cutoff angle depends on a surface wind speed because it is expressed as a function of the wave height and wavelength. Furthermore, the probability that radiation originates from the sea could be dependent on a surface wind speed because the probability distribution of sea surface slope is expressed in terms of a surface wind speed. The advantage of the present method is that the probability that radiation originates from the sea is derived from the probability distribution function of sea surface slope without using a cutoff angle.

It is shown that the calculated sea surface emissivity converges for a practical use by considering up to the first or the second order SESR emissions. Computational results are in good agreement with a Monte Carlo calculations, where the SESR emissivity increases from an emission angle of 50° showing a maximum value of about 0.03 at an emission angle of 80°. The direct emissivity is smaller than the emissivity measurements by Smith et al. (1996) by 0.02∼0.03 around a wavelength of 10 μm at an emission angle of 73.5°. By including the SESR emissivity, the deviation from the measurements is significantly reduced. The algorithm presented in this paper could be extended to the slope distribution model with parameters of wind speed and direction.

Acknowledgements

I would like to thank Yuzo Mano and Hiroshi Ishimoto (MRI) for the useful discussions and the anonymous reviewers for their constructive comments.

References

Bourlier, C. (2005). Unpolarized infrared emissivity with shadow from anisotropic rough sea surface with non-Gaussian statistics. *Applied Optics*, *44*(20), 4335−4349.

Clough, S. A., Shephard, M. W., Mlawer, E. J., Delamere, J. S., Iacono, M. J., Cady-Pereira, K., et al. (2005). Atmospheric radiative transfer modeling: a summary of the AER codes. *Journal of Quantitative Spectroscopy and Radiative Transfer*, *91*, 233−244.

Cox, C., & Munk, W. (1954). Measurement of the roughness of the sea surface from photographs of the sun's glitter. *Journal of the Optical Society of America*, *44*(11), 838−850.

Cox, C., & Munk, W. (1955). Some problems in optical oceanography. *Journal of Marine Research*, *14*(1), 63−78.

Friedman, D. (1969). Infrared characteristics of ocean water (1.5–15 μ). *Applied Optics*, *8*, 2073−2078.

Hale, G. M., & Querry, M. R. (1973). Optical constants of water in the 200-nm to 200 μm wavelength region. *Applied Optics*, *12*, 555−563.

Hanafin, J. A., & Minnett, P. J. (2005). Measurements of the infrared emissivity of a wind-roughened sea surface. *Applied Optics*, *44*(3), 398−411.

Henderson, B. G., Theiler, J., & Villeneuve, P. (2003). The polarized emissivity of a wind-roughened sea surface: A Monte Carlo model. *Remote Sensing of Environment*, *88*, 453−467.

Mano, Y., & Ishimoto, H. (2004). Fast radiative-transfer model based on the correlated *k*-distribibition method for a high-resolution satellite sounder. *Applied Optics*, *43*(34), 6304−6312.

Masuda, K., Takashima, T., & Takayama, Y. (1988). Emissivity of pure and sea waters for the model sea surface in the infrared window regions. *Remote Sensing of Environment*, *24*, 313−329.

Matricardi, M., & Saunders, R. (1999). Fast radiative transfer model for simulation of infrared atmospheric sounding interferometer radiances. *Applied Optics*, *38* (27), 5679−5691.

Saunders, P. M. (1967). Shadowing on the ocean and the existence of the horizon. *Journal of Geophysical Research*, *72*(18), 4643−4649.

Saunders, P. M. (1968). Radiance of sea and sky in the infrared window 800–1200 cm^{-1}. *Journal of the Optical Society of America*, *58*(5), 645−652.

Sherlock, V. (1999). *ISEM-6: Infrared surface emissivity model for RTTOV6.* Forecasting research technical report no.299: Met. Office NWP Division United Kingdom 17 pp.

Smith, W. L., Knuteson, R. O., Revercomb, H. E., Feltz, W., Howell, H. B., Menzel, W. P., et al. (1996). Observations of the infrared radiative properties of the ocean-implications for the measurement of sea surface temperature via satellite remote sensing. *Bulletin of the American Meteorological Society*, *77* (1), 41−51.

Watts, P. D., Allen, M. R., & Nightingale, T. J. (1996). Wind speed effects on sea surface emission and reflection for the Along Track Scanning Radiometer. *Journal of Atmospheric and Oceanic Technology*, *13*(1), 126−141.

Wu, X., & Smith, W. L. (1997). Emissivity of rough sea surface for 8–13 μm: Modeling and validation. *Applied Optics*, *36*(12), 2609−2619.